PERGAMON

Chemical Engineering Science 56 (2001) 4913–4928

Chemical Engineering Science

www.elsevier.com/locate/ces

Gas-assisted non-newtonian fluid displacement in circular tubes and noncircular channels

Fethi Kamişli *, Michael E. Ryan

Department of Chemical Engineering, State University of New York at Buffalo Amherst, NY 14260, USA

Received 25 August 1998; received in revised form 17 March 2001; accepted 6 April 2001

Abstract

The motion of long bubbles into Newtonian and non-Newtonian fluids confined in horizontal circular tubes, rectangular channels, and square cross-sectional channels has been studied both theoretically and experimentally. Of particular interest is the determination of residual liquid film thickness on the walls. Isothermal experiments have been conducted to measure the displacement of the gas–liquid interface as a function of the applied pressure differential. The velocity of the interface and residual liquid film thickness have been determined for both Newtonian and non-Newtonian (shear thinning and viscoelastic) fluids. These experimental results are in good agreement with similar experimental studies conducted by other investigators. The experimental results indicate that the liquid film thickness of constant viscosity viscoelastic fluids (Boger fluids) deposited on the tube wall is thicker than that of comparable Newtonian fluids.

A simple mathematical analysis was developed using a power-law model. The mathematical model successfully captures the gas–liquid dynamics for Newtonian and non-Newtonian fluid displacement in a tube and rectangular channel. The prediction of the liquid fraction deposited on the walls is in qualitative agreement with the experimental observations of previous investigators (Chem. Eng. Sci. 24 (1969) 471; A.I.Ch.E. 16 (1970) 925; Chem. Eng. Sci. 30 (1975) 379). The model gives similar results to a numerical solution (Polm. Eng. Sci. 35 (1995) 877) in which a constitutive equation containing a yield stress is used to model the non-Newtonian behavior. The model is used to determine the location and velocity of the advancing bubble front for the case of a power-law fluid. The results indicate that the gas–liquid interface advances more rapidly with decreasing values of the power-law index above a certain value of dimensionless time ($t/t_b \approx 0.75$).

Keywords: Two-phase flow; Gas-assisted flow; Shear thinning fluid; Viscoelastic fluid

1. Introduction

The motion of long bubbles into Newtonian fluids confined in horizontal cylindrical tubes or channels of rectangular cross-section (Hele–Shaw cell) has been studied for several years. When a less viscous fluid displaces a more viscous fluid from the gap between two closely-spaced parallel plates, the interface develops a tongue-like shape with the less viscous fluid penetrating into the more viscous fluid. Similarly, when air is forced into one end of a circular tube containing a viscous liquid, it forms a round-ended column or bullet-like shape which travels down the tube forcing some liquid out at the far end and leaving a fraction of the liquid m, in the form of an annular layer covering the wall. In the case of a square channel the shape of the less viscous fluid penetrating into the more viscous fluid depends on the velocity of the penetrating fluid. If the velocity of the penetrating fluid (called the bubble or finger hereafter) is larger than a certain limiting value, the bubble assumes a bullet-like shape; otherwise, the bubble conforms to the shape of the square channel. In a rectangular channel, if the capillary number, $\mathrm{Ca} = \mu u_b/\sigma$ is not too large, a single steady-state tongue-like shape moves through the cell with constant velocity u_b, where μ is the viscosity of the driven liquid, u_b is the bubble velocity, and σ is the gas–liquid interfacial tension. In a

* Corresponding author. Department of Chemical Engineering, Faculty of Engineering, University of Firat, Elazig 23279, Turkey.
E-mail address: fkamisli@firat.edu.tr (F. Kamişli).

0009-2509/01/$ - see front matter
PII: S0009-2509(01)00136-1

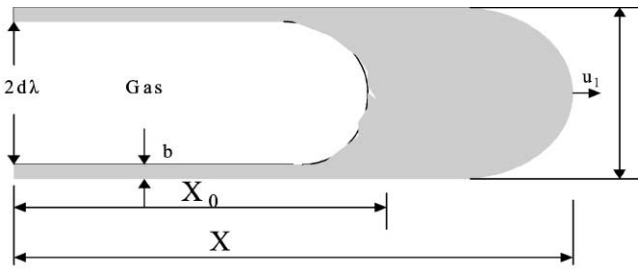

Fig. 1. Schematic diagram of gas-assisted displacement.

circular tube or square channel the bullet-like shape of the bubble persists even at a very large capillary number. In other words, the fingering effect does not occur in the case of a long bubble advancing in either a circular tube or a square channel at large capillary numbers.

A similar two-phase flow occurs in gas-assisted injection molding, a process for fabricating hollow thermoplastic parts in which the injection of molten plastic into a mold is assisted by pressurized gas. Because the pressure is transmitted through the inviscid gas with minimal losses, parts can be fabricated with lower clamping force and with a more uniform pressure distribution than in conventional injection molding.

In recent years there has been a considerable interest shown in gas-assisted injection molding. This molding process offers a cost-effective means of production of hollow plastic parts. The process has resolved many problems associated with conventional injection molding such as reduction in warpage and elimination of sink marks. It also offers other benefits such as high rigidity, reduction in clamp force, part weight reduction, cycle time reduction, improved surface finish and permitting the design of parts with variable wall thickness.

In general, gas-assisted injection molding can be described by four consecutive stages (see Poslinski et al., 1995). The first stage consists of the familiar fountain flow. The second stage (primary gas penetration) is the principal subject of this paper and is also encountered in other industrial operations such as oil recovery and the coating of monolithic structures for the manufacture of automotive catalytic converters.

Four distinct flow regions can be identified during primary gas penetration (see Fig. 1); the advancing melt front, the deforming viscous melt, the penetrating gas front, and the stagnant material already hollowed out by the gas. The first two regions are identical to conventional mold filling. Because the ratio of the part thickness to the overall size of the molded plastic part is normally much less than unity, the bulk of the deformation can be described by balancing the pressure gradient in the flow direction with the shear stress variation across the thickness direction. In order to complete a more rigorous analysis, the influence of secondary flows near the melt and gas fronts need to be included.

The numerical techniques which have been well developed by Kamal, Goal, and Chu (1988), Friedrichs and Güç eri (1993), and others for conventional injection mold filling can be used for analyzing the melt front region in gas-assisted injection mold filling without modification. However, these analyses needs to be modified in order to model the gas-molten polymer interface associated with gas-assisted injection molding.

The bubble front region is important in the gas-assisted displacement process especially in rectangular channels since Saffman and Taylor (1958), Pitts (1980), Tabeling, Zocchi, and Libchaber (1987), and others, experimentally observed that instability of the gas front (fingering) occurs as the bubble velocity is increased. The bubble velocity depends on the pressure of the gas, and determines the extent of penetration and the resulting wall thickness of gas-assisted molded parts.

The study of gas-assisted displacement of Newtonian fluids in circular tubes and rectangular channels is relevant for determining the film thickness, bubble shape, and stability of the process and has been investigated extensively. Koelling and Kaminski (1996) studied experimentally gas-assisted injection molding for several molten polymers (polystyrene, polyvinyl chloride, and polycarbonate). They reported that the wall thickness along the gas flow path is a strong function of residual time, gas bubble velocity, and material rheology. The residual time is defined for each point on the flow path of the gas bubble as the difference in time between the passing polymer melt front and the moving bubble tip. There is no well established numerical technique to predict the wall thickness distribution and location of the gas front region associated with gas-assisted injection molding. An accurate prediction of these two quantities is important for evaluating the structural performance of the finished product. Some investigators (see Turng & Wang, 1991; Turng, 1993) have claimed that they have developed a numerical technique capable of determining the wall thickness and front region; on the other hand, other investigators (see Moritzer & Potente, 1996; Poslinski et al., 1995) have indicated that current numerical techniques lack the capability to accurately determine the wall thickness and gas front location. The determination of the wall thickness, the secondary gas penetration, and the gas front location still requires additional research. As mentioned previously, gas-assisted liquid displacement, has been extensively investigated for more than sixty years. Fairbrother and Stubbs (1935) performed the first experiments to determine the amount of liquid left inside a tube when it is displaced by another immiscible fluid. They determined the flow rate of the liquid by measuring the motion of the gas interface in the tube. An empirical correlation for the fraction of the liquid deposited on the walls of the tube was formulated as follows:

$$m = (u_b - u)/u_b = 1.0\ \mathrm{Ca}^{1/2} = (\mu u_b/\sigma)^{1/2}. \quad (1)$$

This result was found satisfactory for capillary numbers between 10^{-3} and 10^{-2}. When the tube is not completely filled with the test liquid and open to the atmosphere, the gas interface will move faster than the average velocity of the liquid due to the deposition of a thin film of liquid on the walls of the tube. If the tube is long enough, blowout will take place somewhere within the tube.

Isothermal gas-assisted displacement of Newtonian liquids in circular tubes was also experimentally studied by Taylor (1961). By plotting the fraction of the liquid as a function of the capillary number, he collapsed the data onto a single curve, and showed that this fraction asymptotically approached the value of 0.56 for a capillary number nearly equal to 2. Cox (1962, 1964) extended Taylor's result to capillary numbers up to 10 and showed that the limiting fraction of the liquid deposited on the walls of the tube was approximately 0.6. His theoretical analysis resulted in a fourth-order differential equation in terms of the stream function. Inertial and gravitational forces were neglected. The streamlines were assumed to be a specific function of the spatial coordinates. The governing equations were expressed in a matrix form and solved numerically.

Bretherton (1961) also undertook a theoretical analysis of this problem for circular capillaries. He found an approximate solution using the method of matched asymptotic expansions. The idea behind this theoretical treatment is that for sufficiently small Ca the viscous stresses appreciably modify the static profile of the bubble only very near to the wall. In this region, the *lubrication approximation* gives a good description of the flow field and of the interface profile. Using the lubrication approximation which requires quasi-unidirectional flow in the thin liquid film and assuming the slope of the fluid–fluid interface to be small, it can be shown that the velocity profile is parabolic. The bubble is assumed to be inviscid resulting in a constant pressure within the bubble. The pressure in the liquid film is given by the pressure drop across the interface which is approximated by the Young–Laplace equation. Bretherton (1961) also systematically explored a number of possible causes for the discrepancy between the analysis and experimental data. Schwart, Princen, and Kiss (1986) considered the same problem and found some differences in liquid film thickness for sufficiently long bubbles, as compared to short bubbles.

An experimental study by Marchessault and Mason (1960) used air bubbles in a dilute aqueous solution of potassium chloride. Film thicknesses were inferred from resistance measurements and were found to be substantially larger than those reported by Bretherton. The residual wetting layer of the displaced liquid will vary with the velocity of advance of the interface. Numerical studies of capillary-tube displacement of a wetting liquid by a semi-infinite inviscid slug of gas have been presented. Both Reinelt and Saffman (1985) using a finite-difference method and Shen and Udell (1985) using a finite element approach solved the full creeping-motion equations with the continuity of stress imposed exactly on the free surface.

Ratulowski and Chang (1989) investigated a single discrete bubble and the motion of a long bubble in a circular tube and square channel. They determined the fraction of liquid deposited on the walls of the tube or channel and the pressure drop across the bubble front. According to their study, a single isolated bubble resembles an infinitely long bubble in terms of determining the film thickness and pressure drop across the bubble front if the length of the bubble exceeds the channel width. Their analysis is only valid for $Ca > 3 \times 10^{-3}$.

The flow of invicid bubbles and viscous drops in capillary tubes has been theoretically studied by Westborg and Hassager (1989) using a Galerkin finite element method. They indicated that the results of simulation show good agreement with published experimental data.

Kolb and Cerro (1991) studied the isothermal gas-assisted displacement of a Newtonian liquid from a channel of square cross-section and showed that the liquid deposited on the wall of the square tube also approaches an asymptotic limit at high capillary numbers. Above $Ca = 0.1$, the gas forms a circular hollow core and thicker liquid deposition; below $Ca = 0.1$, the hollow core takes on the square cross-section of the tube as the deposition thickness is reduced. The above study was extended (Kolb & Cerro, 1993) by adding the *lubrication approximation* for intermediate to large capillary numbers where the flow is axisymmetric. In their work the film thickness on the walls of the square channel can be predicted as a function of capillary number since the velocity profile of the fluid flowing between the bubble and the square channel walls is known. It was claimed that the *lubrication approximation* solution is in good agreement with experimental data for values of capillary numbers between 0.7 and 2.0.

Unlike previous investigators, Poslinski et al. (1995) investigated non-Newtonian fluids deposited on the walls of a tube. They found that the fraction of the non-Newtonian fluid deposited on the walls is less than that of a corresponding Newtonian fluid at a low capillary number. At a higher capillary number the fraction of the liquid deposited asymptotically increases and approaches a value of 0.58.

Ro and Homsy (1995) performed an asymptotic analysis of the gas-assisted displacement of a non-Newtonian fluid in a Hele–Shaw cell. The effects of normal stress and shear stress thinning in determining the film thickness and the pressure jump across the interface were examined. Viscoelastic fluids were modeled by an Oldroyd-B constitutive equation and the solutions for the constant film thickness region and the static meniscus region were matched in the transition regime as for the Newtonian case (see Park & Homsy, 1984).

The planar geometry or Hele–Shaw cell consists of two closely-separated parallel plates having a distance $2d$ between them. The sides of this rectangular channel are at a distance $2Z_0$ apart where $d \ll Z_0$ parameter λ is defined as (thickness of gas bubble)/(distance between the plates). For the cylindrical tube λ is defined as (diameter of the bubble)/(diameter of the tube). In the rectangular channel the thickness of the tongue-like shape is $2\lambda d$ and its width is $2\lambda_w Z_0$, where the parameter λ_w is equal to (width of the bubble)/(width of the rectangular channel).

The determination of the value of λ and λ_w has been a subject of much interest. The determination of λ_w as a function of capillary number Ca, for different cell aspect ratios, Z_0/d, has been examined experimentally by Saffman and Taylor (1958), Pitts (1980), and Tabeling et al. (1987). Saffman and Taylor (1958) and Pitts (1980) found that the value of λ_w decreases monotonically to 0.5 when the bubble velocity is increased. In contrast, Tabeling et al. (1987) reported that the value of λ_w never decreases to 0.5 when the bubble velocity is increased. The problem was reconsidered by McLean and Saffman (1981) by including surface tension effects due to the lateral curvature of the interface of the advancing finger. In their numerical study the value of λ_w was close to 0.5 at large bubble velocity which is in good agreement with the experimental data. At low velocities (i.e. $C_b = 12\ \mathrm{Ca}(Z_0/d)^2 < 100$), the agreement with the experiment was ambiguous since the finger sizes predicted by the theory were significantly below those actually measured. They found that the incorporation of surface tension and cell aspect ratio did not remedy or reduce the disagreement between theory and experiment in terms of calculating the value of λ_w as a function of C_b. The approach of Bretherton (1961) was reconsidered by Park and Homsy (1984) in the horizontal Hele–Shaw cell at a very low capillary number. The problem was solved using a perturbation method with an asymptotic expansion of $\mathrm{Ca}^{1/3}$ and the ratio of the gap width to the transverse characteristic length $\delta_e = d/Z_0$ as small quantities. They obtained relationships between λ, Ca, and δ_e for calculating the film thickness and pressure jump across the bubble front. The resulting expressions were compared with the results of Bretherton (1961) and Landau and Levich (1942) and were considered to give improved results.

Reinelt (1987a) extended his earlier work by determining the perturbation solution of the axisymmetric flow problem for small values of Ca and $\delta = d/R$. In his study, some of the boundary conditions were improved by incorporating the film thickness into the kinematic boundary condition and taking into account the dependence of Δp on the capillary number. The problem was also numerically solved using a conformal mapping method and the numerical results were presented in another paper (Reinelt, 1987b).

Huzyak and Koelling (1997) experimentally investigated the gas-assisted displacement of non-Newtonian fluids deposited on the walls of a tube. They examined the effect of fluid elasticity and tube diameter on the fractional coverage. They concluded that unlike Newtonian fluids, the fractional coverage for viscoelastic fluids did not reach an asymptotic value but continued to increase, attaining a value in excess of 0.75 and that the fractional coverage of viscoelastic fluids decreases with increasing tube diameter.

In a recent study, Chen, Hu, Jong, and Jeng (1997) indicated that a complete computer-aided engineering (CAE) package of the entire gas-assisted injection molding process is not available at the present time. They developed a unified CAE model using ANSYS and claimed that it can be used for structural analysis, process simulation, and warpage calculations for a gas-assisted injection molded part. Another simulation was recently developed by Chang, Tsai, and Hsu (1997) and was applied to the analysis of the gas-assisted injection molding process. Dynamic animation of the results was utilized to mimic the dynamics of the polymer melt, gas injection and gas penetration behavior during filling and packing. However, their simulation did not allow them to examine the interaction of fluid flow and heat transfer, where secondary gas penetration takes place.

Soh and Chung (1997) performed experiments for determining the flow direction of a long bubble in the gas-assisted injection molding process. In their study, gas was injected into a molten polymer and the flow direction was observed experimentally. They examined different initially filled lengths from the gas injection point, two different diameter tubes, and two different geometries. Although the non-Newtonian polymer was modeled as a Newtonian fluid, the experimental observations were in qualitatively good agreement with the simulation. They concluded that the gas always preferred the direction of least resistance which coincides with the pressure drop in the axial direction.

Although some studies have included non-Newtonian or viscoelastic fluids, the effects of shear thinning, normal stresses, and viscoelasticity on the liquid film thickness require further experimental and theoretical investigation. Although some experiments were performed using a shear thinning and viscoelastic fluid by Huzyak and Koelling (1994), the effects of shear thinning and elasticity of fluid were not clearly differentiated.

The primary purpose of the present study was to visualize the dynamics of gas penetration into non-Newtonian fluids and to characterize the part thickness around the hollow core (fraction of liquid deposited on the walls of the mold) as a function of the fluid rheology. Also, the effects of steady state and unsteady bubble velocity on the liquid film thickness were experimentally investigated. The experimental results will provide insight into the gas–liquid dynamics during the displacement process.

2. Gas–liquid dynamics for non-Newtonian fluids in gas-assisted displacement

When gas is injected into a partially filled circular (or rectangular) horizontal channel at the filled end of the channel, the moving bubble assumes its final bullet-like shape within a distance of a few tube diameters and the motion pushes some of the liquid towards the far end of the tube. If the tube is long enough, blowout takes place within the tube or channel. In general, the velocity of the long gas bubble depends upon the process variables such as the gas pressure, the initially filled liquid length, the tube diameter (or distance between the plates), and the amount of liquid between the bubble front and the liquid front. If all other parameters are kept constant except for the amount of liquid between the bubble front and the liquid front (which must decrease with time or otherwise the coating thickness on the wall would not exist) the velocity of the bubble will necessarily change as a function of the amount of liquid between these two points.

Consider the case of liquid displacement confined in a horizontal tube or channel. For the case of displacement between two flat, parallel, closely seperated horizontal plates, a two-dimensional approximation to the flow is valid. The equations of continuity and motion for an incompressible Newtonian or non-Newtonian fluid are given by

$$\frac{1}{\dot{y}^a}\frac{\partial}{\partial \dot{y}}(\dot{y}^a \dot{u}) + \frac{\partial \dot{v}}{\partial \dot{x}} = 0, \tag{2}$$

$$\rho\left(\frac{\partial \dot{v}}{\partial \dot{t}} + \dot{v}\frac{\partial \dot{v}}{\partial \dot{x}} + \dot{u}\frac{\partial \dot{v}}{\partial \dot{y}}\right) = -\frac{\partial \dot{p}}{\partial \dot{x}} - \left[\frac{1}{\dot{y}^a}\frac{\partial}{\partial \dot{y}}(\dot{y}^a \tau_{yx}) + \frac{\partial \tau_{xx}}{\partial \dot{x}}\right], \tag{3}$$

$$\rho\left(\frac{\partial \dot{u}}{\partial \dot{t}} + \dot{v}\frac{\partial \dot{v}}{\partial \dot{x}} + \dot{u}\frac{\partial \dot{u}}{\partial \dot{y}}\right) = -\frac{\partial \dot{p}}{\partial \dot{y}} - \left[\frac{1}{\dot{y}^a}\frac{\partial}{\partial \dot{y}}(\dot{y}^a \tau_{yy}) + \frac{\partial \tau_{xy}}{\partial \dot{x}}\right]. \tag{4}$$

The parameter a has a value of either 0 or 1 depending on the geometry (0 corresponds to the planar case and 1 corresponds to a cylindrical geometry). τ_{ij} is the stress tensor and $\dot{p}$ is the pressure. The velocity components $\dot{v}$ and $\dot{u}$ are in the $\dot{x}$ and $\dot{y}$ directions, respectively. The $\dot{y}$ axis is taken normal to the channel plates (or tube wall) with the origin at the mid-plane (or tube axis). Thus $\dot{y}$ has the value of $\pm d$ for the planar case (or d for the cylindrical case) at the solid boundaries.

3. Gas–liquid dynamics for a circular tube

In this analysis of the gas-assisted displacement process, a power-law model is used in order to derive the equations describing the gas–liquid dynamics of a non-Newtonian fluid. Following the analysis of Poslinski et al. (1995), a simple model for the displacement process in a cylindrical tube, or other geometry, can be derived by neglecting the curvature of the interface. The total liquid to be displaced is $\pi d^2 X_0$ for a cylindrical tube and $4dX_0Z_0$ for a rectangular channel, where d denotes either the radius of the tube or mid-plane distance to the wall of the channel, X_0 is the initial length of liquid in the axial direction, and Z_0 is the half width of the channel (see Fig. 1). At time $t = 0$ a pressurized gas is injected at $x = 0$, the filled end of the tube, in order to initiate the gas-assisted displacement process. The pressure difference $\Delta p_a = p_g - p_a$ results in the formation of a long bubble in the tube or channel causing displacement of the liquid, where p_g is the applied gas pressure and p_a is the ambient pressure. At any instant t_l; X, L and u_l, u_b indicate the average positions and average velocities of the liquid front and the bubble front, respectively. When the bubble moves forward in the tube, a deposited liquid layer of thickness b remains on the walls of the tube or channel. The fraction of the liquid deposited on the walls of the tube is given by

$$m = 1 - \frac{1}{L}\int_0^L (1-E)^2 \,\mathrm{d}x, \tag{5}$$

where the thickness ratio $E = b/d$ is, in general, a function of the axial length x. In the limiting case of $b = 0$, the gas bubble completely fills the entire tube and the liquid velocity becomes equal to the bubble velocity and blowout never takes place within the tube. This case is only possible where perfect slip exists along the tube wall. For $b > 0$, the distance between the liquid front and the bubble front $X - L$ continually decreases with time. An unhindered motion then causes blowout of the gas through the liquid front at $t = t_b$ and $X = L_b$. The blowout ratio L_b/X_0 characterizes the distance traveled by the liquid front relative to its initial axial position.

A mass balance expression can be written as follows:

$$X - X_0 = \int_0^L (1-E)^2 \,\mathrm{d}x. \tag{6}$$

Combining Eqs. (5) and (6) gives

$$X - X_0 = (1-m)L = \int_0^L (1-E)^2 \,\mathrm{d}x. \tag{7}$$

According to this expression the blowout position $X = L = L_b$ is solely determined by the initial liquid length and the coating volume fraction, i.e. $L_b = X_0/m$. The liquid thickness does not change with time once it is formed by the advancing gas front. Although E, in general, depends on the position of the bubble L, it does not explicitly depend on time. In other words, the value of E at a particular location within the tube will not change with time.

After integration of Eq. (6) assuming that E does not change with axial position of the bubble, the result equation is differentiated with respect to time in order to

obtain the relationships between the velocity of the liquid front and bubble front and the resulting equation is

$$\frac{\mathrm{d}X}{\mathrm{d}t} = (1 - E(L))^2 \frac{\mathrm{d}L}{\mathrm{d}t}. \tag{8}$$

As can be seen from Eq. (8) for the limiting case $E = 0$, the liquid front and bubble front move with the same average velocity and during the displacement the distance between these two points $X - L$ remains unchanged from the initial value of X_0. As a result blowout will never occur within the tube. Since the liquid is deposited on the wall of the tube $E > 0$, $X - L$ continually diminishes with time and the gas penetration rate increases by a factor $1/(1 - E(L))^2$. If it is assumed that the bubble takes its final shape within a few tube diameters, Eq. (8) can be written as follows:

$$\frac{\mathrm{d}X}{\mathrm{d}t} = (1 - E_\infty)^2 \frac{\mathrm{d}L}{\mathrm{d}t}. \tag{9}$$

An analytical solution at high bubble velocities can be obtained by assuming that the gas pressure reaches its final value instantaneously and remains fixed during the entire displacement process. Under these conditions, the thickness ratio has a constant value of E_∞.

The average liquid velocity can also be obtained from the equation of motion for steady tube flow using a power-law model for a non-Newtonian fluid. In this approach the frame of reference is taken with respect to the stationary walls of the tube or channel. In order to nondimensionalize the governing equations, the scaling factors are chosen accordingly and the relevant dimensionless quantities are defined as follows:

$$v = \frac{\dot{v}}{u_i}, \quad u = \frac{\dot{u}L_b}{u_i d}, \quad y = \frac{\dot{y}}{d}, \quad Re = \frac{\rho u_i d^2}{ML_b}$$

$$x = \frac{\dot{x}}{L_b}, \quad p = \frac{\dot{p}}{P}, \quad P = \frac{Mu_i L_b}{d^2}, \quad t = \frac{\dot{t}u_i}{L_b},$$

where L_b is the blowout length, u_i is the initial bubble velocity, and M is an apparent viscosity. For the circular tube (a is taken to be equal to 1) Eqs. (3) and (4) become

$$Re\left(\frac{\partial v}{\partial t} + v\frac{\partial v}{\partial x} + u\frac{\partial v}{\partial y}\right) = -\frac{\partial p}{\partial x} + \frac{1}{y}\frac{\partial}{\partial y}\left[\mu y\left(\left(\frac{d}{L_b}\right)^2 \frac{\partial u}{\partial x} + \frac{\partial v}{\partial y}\right)\right] + \left(\frac{d}{L_b}\right)^2 \frac{\partial}{\partial x}\left(2\mu\frac{\partial v}{\partial x}\right),$$

$$Re\left(\frac{d}{L_b}\right)^2\left(\frac{\partial u}{\partial t} + v\frac{\partial u}{\partial x} + u\frac{\partial u}{\partial y}\right) = -\frac{\partial p}{\partial y} + \left(\frac{d}{L_b}\right)^2\left\{\frac{1}{y}\frac{\partial}{\partial y}\left(2\mu\frac{\partial u}{\partial y}\right) + \frac{\partial}{\partial x}\left[\mu\left(\left(\frac{d}{L_b}\right)^2\frac{\partial u}{\partial x} + \frac{\partial v}{\partial y}\right)\right]\right\}.$$

In the gas-assisted displacement process, the inertia terms are negligible compared with the viscous terms. Thus, Re and $(d/L_b)^2$ are very small in comparison with unity. For $Re \ll 1$ and $(d/L_b)^2 \ll 1$ the above equations become

$$\frac{\partial p}{\partial x} = \frac{1}{y}\frac{\partial}{\partial y}\left(\mu y\frac{\partial v}{\partial y}\right), \tag{10}$$

$$\frac{\partial p}{\partial y} = 0, \tag{11}$$

where μ is the viscosity of the liquid which depends on the rate of strain for a non-Newtonian fluid. In this analysis, a power-law model is considered where the viscosity is defined as

$$\dot{\mu} = K(II_\Delta)^{(n-1/2)}$$

and

$$\Delta = \begin{bmatrix} 2\dfrac{\partial \dot{v}}{\partial \dot{x}} & \dfrac{\partial \dot{u}}{\partial \dot{x}} + \dfrac{\partial \dot{v}}{\partial \dot{y}} \\ \dfrac{\partial \dot{u}}{\partial \dot{x}} + \dfrac{\partial \dot{v}}{\partial \dot{y}} & 2\dfrac{\partial \dot{u}}{\partial \dot{y}} \end{bmatrix}.$$

The second scalar invariant is

$$II_\Delta = 4\left(\frac{\partial \dot{v}}{\partial \dot{x}}\right)^2 + 2\left(\frac{\partial \dot{u}}{\partial \dot{x}} + \frac{\partial \dot{v}}{\partial \dot{y}}\right)^2 + 4\left(\frac{\partial \dot{u}}{\partial \dot{y}}\right)^2.$$

Thus μ in a dimensionless form for a power-law fluid is given by

$$\mu = K\left(\frac{u_i}{d}\right)^{n-1}\left[2\left(\frac{d}{L_b}\right)^2\left(\left(\frac{\partial v}{\partial x}\right)^2 + \left(\frac{\partial u}{\partial y}\right)^2\right) + \left(\left(\frac{d}{L_b}\right)^2\frac{\partial u}{\partial x} + \frac{\partial v}{\partial y}\right)^2\right]^{(n-1/2)}.$$

When $(d/L_b) \ll 1$ the above equation becomes

$$\mu = M\left|\frac{\partial v}{\partial y}\right|^{n-1},$$

where $M = (u_i/d)^{n-1}$ can be considered as the apparent viscosity at a (nominal) shear rate of (u_i/d). Since $\partial v/\partial y < 0$ for all y in tubular flow and when $\Delta p/\Delta x < 0$ the average liquid velocity for a power-law fluid is given by

$$\bar{v} = \frac{d^{\alpha+1}}{\alpha + 3}\left[\frac{1}{2M}\frac{\partial p}{\partial x}\right]^\alpha, \tag{12}$$

where $\alpha = 1/n$. Eq. (12) is obtained subject to the boundary conditions $\partial v/\partial y = 0$. An analytical solution at high bubble velocities can be obtained by assuming that the gas pressure reaches its final value instantaneously and remains fixed during the entire displacement process, i.e. $\Delta Pg = \Delta Pa(\Delta Pg = \mathrm{Pg} - \mathrm{Pa},\ \Delta Pa = \mathrm{P} - \mathrm{Pa};\ Pg$: gas pressure, P: pressure from fluid flow, and Pa: ambient pressure). Therefore, taking $\partial p/\partial x = \Delta p_a/(X - L)$ in Eq. (12) and substituting into Eq. (9) gives

$$(1 - E_\infty)^2 \frac{\mathrm{d}L}{\mathrm{d}t} = \frac{d^{\alpha+1}}{\alpha + 3}\left[\frac{1}{2M}\frac{\Delta p}{(X - L)}\right]^\alpha \tag{13}$$

combining Eqs. (7) and (13) and the resulted equation integrated with respect to t from 0 to t_b and L from 0 to L_b gives

$$\frac{1}{\alpha + 1}[X_0^{\alpha+1} - (X_0 - mL_b)^{\alpha+1}] = \frac{md^{\alpha+1}}{(1 - m)(\alpha + 3)}\left(\frac{\Delta p_a}{2M}\right)^\alpha t_b, \tag{14}$$

where t_b is the blowout time. The initial velocity u_i, is defined as L_b/t_b and is given by

$$u_i = \frac{1}{1 - m}\left(\frac{\alpha + 1}{\alpha + 3}\right)\frac{d^{\alpha+1}}{X_0^\alpha}\left(\frac{\Delta p_a}{2M}\right)^\alpha. \tag{15}$$

The blowout time can be found by substituting $L_b = X_0/m$ into Eq. (14)

$$t_b = \frac{1 - m}{m}\left(\frac{\alpha + 3}{\alpha + 1}\right)\left(\frac{X_0}{d}\right)^{\alpha+1}\left(\frac{\Delta p_a}{2M}\right)^{-\alpha}. \tag{16}$$

This expression shows the influence of the process variables on the isothermal gas-assisted displacement process. As can be seen, a higher viscosity M, and a larger amount of liquid to be displaced, X_0, increases the flow resistance thereby reducing the bubble velocity and delaying blowout. A higher gas pressure and a larger cross-sectional flow area facilitate the displacement process. The power-law index also influences the displacement process. From the above equation an increase in the power-law index will reduce the flow resistance thereby increasing the bubble velocity and diminishing the blowout time. In order to make this point clear, the blowout time is plotted as a function of pressure drop for various values of the power-law index in Fig. 2. M and m were taken to be constant in equation for evaluating the blowout time. In general, m depends on Δp, M, and the power-law index (the variation in m and M will affect the process in a similar way). M also depends upon the power-law index. Therefore no attempt was made to compare this result quantitatively with the experimental data even though the computed results from Eq. (16) were found to be in quantitative agreement with the experimental data for a Newtonian fluid. As can be seen in Fig. 2, the blowout time increases with decreasing power-law index thereby decreasing the bubble velocity. A similar trend was also observed experimentally.

After some manipulations, normalized bubble front and liquid front, respectively, are obtained as follows.

$$\frac{L}{L_b} = 1 - \left(1 - \frac{t}{t_b}\right)^{1/\alpha+1}, \tag{17}$$

$$\frac{X}{L_b} = 1 - (1 - m)\left(1 - \frac{t}{t_b}\right)^{1/\alpha+1}. \tag{18}$$

The liquid front and the bubble front velocities can be obtained by differentiating Eqs. (18) and (17) directly. Thus

$$\frac{u_l}{u_i} = \frac{1 - m}{\alpha + 1}\left(1 - \frac{t}{t_b}\right)^{-(\alpha/\alpha+1)}, \tag{19}$$

$$\frac{u_b}{u_i} = \frac{1}{\alpha + 1}\left(1 - \frac{t}{t_b}\right)^{-(\alpha/\alpha+1)}. \tag{20}$$

During the gas-assisted displacement process, the bubble position, the liquid front, and the liquid and bubble velocities can be calculated analytically from Eqs. (17)–(20), respectively. The corresponding expressions for a Newtonian fluid ($n = 1$) have been given by Poslinski et al. (1995). Although viscoplastic fluids were examined experimentally in their paper, the theoretical analysis was obtained with the assumption that the fluid is Newtonian.

X/L_b, L/L_b, t/t_b can be considered as the normalized liquid front position, bubble front position, and normalized time, respectively. These variables and the liquid front and bubble front velocities are evaluated from the above analytical solution for different values of n as shown in Fig. 3. Blowout always takes place at $L/L_b = 1$ and $t/t_b = 1$. Although the liquid front and bubble velocities are divided by the average velocity, blowout does not occur at $u_l/u_i = 1$ or $u_b/u_i = 1$ since the liquid front and bubble front velocity exceed the average velocity at some position within the tube.

4. Gas–liquid dynamics for a rectangular channel

A simple model for the gas-assisted displacement in a rectangular or square channel can also be derived by neglecting the curvature of the interface. The mass balance requires that the initially filled liquid to be displaced must be equal to the liquid deposited on the walls of the rectangular or square tube plus the displaced liquid downstream of the gas front. The initially filled liquid volume is equal to $4Z_0X_0d$. All symbols are the same as previously defined. The following equations can be written from material balance considerations.

$$m = \frac{1}{L}\int_0^L E\,\mathrm{d}x, \tag{21}$$

$$X - X_0 = L - \int_0^L E\,\mathrm{d}x. \tag{22}$$

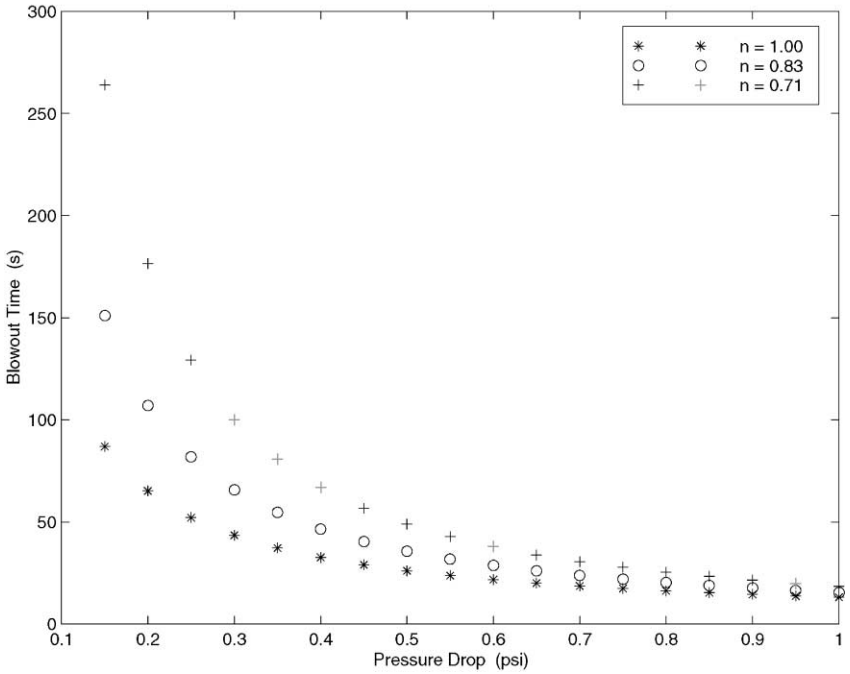

Fig. 2. Effect of power-law index on the blowout time.

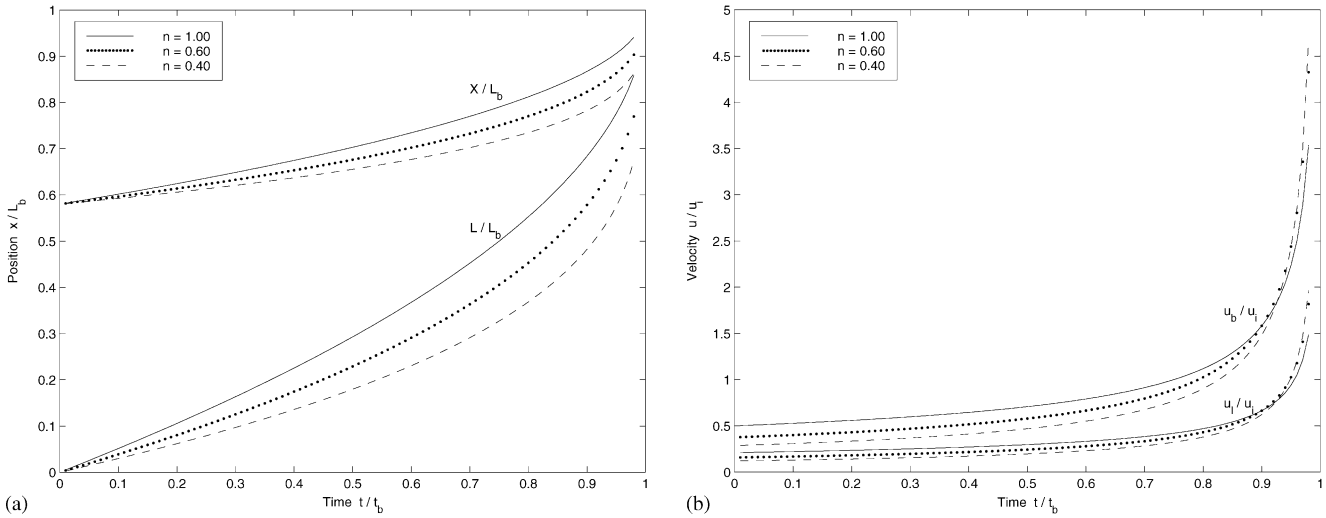

Fig. 3. Analytical predictions for (a) liquid front and bubble front position and (b) velocity as a function of normalized time with power-law index as a parameter.

Here E becomes equal to m for the planar case when edge effects are neglected, where $E = b/d$ and $m = 1 - \lambda$. If the same procedure outlined in the previous section for the cylindrical tube is followed, the following expressions result:

$$u_i = \frac{1}{1-m}\left(\frac{\alpha+1}{\alpha+2}\right)\frac{d^{\alpha+1}}{X_0^{\alpha}}\left(\frac{\Delta p_a}{2M}\right)^{\alpha}, \tag{23}$$

$$t_b = \frac{1-m}{m}\left(\frac{\alpha+2}{\alpha+1}\right)\left(\frac{X_0}{d}\right)^{\alpha+1}\left(\frac{\Delta p_a}{2M}\right)^{-\alpha}, \tag{24}$$

$$\frac{L}{L_b} = 1 - \left(1 - \frac{t}{t_b}\right)^{1/\alpha+1}, \tag{25}$$

$$\frac{X}{L_b} = 1 - (1-m)\left(1 - \frac{t}{t_b}\right)^{1/\alpha+1}, \tag{26}$$

$$\frac{u_l}{u_i} = \frac{1-m}{\alpha+1}\left(1 - \frac{t}{t_b}\right)^{-\alpha/\alpha+1}, \tag{27}$$

$$\frac{u_b}{u_i} = \frac{1}{\alpha+1}\left(1 - \frac{t}{t_b}\right)^{-(\alpha/\alpha+1)}. \tag{28}$$

Although the form of the coefficients in the expressions for the initial velocity and blowout time depend on the channel geometry, the time dependence of the liquid and bubble front position and velocities are the same.

In gas-assisted displacement, these simple models indicate that the deposited liquid thickness on the walls of the tube or channel decreases with decreasing power-law index as shown in Fig. 3a. This result qualitatively agrees with the experimental data of previous investigators (Tallmadge, 1969, 1970; Spiers et al., 1975). These investigators report that non-Newtonian fluids give a smaller film thickness than for a corresponding Newtonian fluid on a plate or belt associated with the free coating process.

The thinner liquid deposited on the walls of the tube or channel results in a larger amount of liquid being displaced, adding to the flow resistance, thus impeding the gas penetration. For all values of n, the interface velocity starts to increase slowly in the early stages of gas penetration and rises rapidly after $t/t_b \approx 0.7$ as shown in Fig. 3b.

From the simple mathematical model, the liquid and bubble position and the liquid and bubble front velocity can be calculated analytically as a function of dimensionless time for various values of the power-law index. From this model, the fractional coverage of liquid can be estimated by considering the liquid and bubble front position as a function of the power-law index. As expressed earlier, the fraction of the liquid deposited on the wall decreases with decreasing power-law index.

5. Experimental

The motion of a long gas bubble into Newtonian and non-Newtonian fluids confined in horizontal circular and square cross-section channels (gas-assisted liquid displacement) has been studied experimentally. Of particular interest is the determination of the residual liquid film thickness on the walls of the tube or channel. Isothermal experiments have been conducted to measure the displacement of the gas–liquid interface as a function of the applied pressure differential. The velocity of the interface and the residual liquid film thickness have been determined for both Newtonian, non-Newtonian (shear thinning), and viscoelastic liquids.

Experiments were performed in two types of tube arrangements namely open tubes and valve-mounted closed tubes. In the gas-assisted injection molding process, during mold filling and primary gas penetration, the molten polymer does not encounter any additional resistance except flow resistance until the mold is completely filled. Therefore, most experiments were conducted using tubes open to the atmosphere. The valve-mounted closed tubes result in a uniform bubble velocity since the flow resistance of the fluid in the channel is negligible when compared with the resistance due to the valve. In order to compare the amount of residual liquid on the wall which is obtained from open tubes, experiments were also conducted using a valve-mounted closed tube.

6. Apparatus

The experimental arrangement consisted of a gas supply tank, pressure transducer, transparent plastic or glass tubes/channels and associated valves and fittings as shown in Fig. 4. The volume of the gas supply tank (diameter: 14 cm and length: 25 cm) was chosen to be very large in comparison to the volume of the gas within the tube or channel in order to minimize pressure fluctuations during the experiments. Pressurized air was used and was supplied by a local compressed air line and monitored with a pressure gauge mounted on the tank. The desired pressure level can be accurately adjusted by keeping valve B open and valve D closed and reading the pressure from the pressure transducer for a particular setting of valve C. The line pressure is also independently measured using a pressure transducer situated close to the channel assembly. Plastic or glass tubes having four different diameters (3.17, 4.76, 6.35, and 9.52 mm) and a length of 50 cm were used. Caliper measurements showed that the inner radius along the tube length had a maximum variation of ± 0.065 mm. The length of the tube chosen is long enough such that blowout occurs within the length of the tube for the applied pressure. As expected a low gas pressure requires that a long tube be used in order for blowout to take place within the tube.

Experiments were performed using both Newtonian and non-Newtonian liquids. Corn syrup, hydroxyethylcellulose HEC (99-250 MR), carboxymethylcellulose CMC (99-7 HF), and polyacrylamide PAA (percol 336) were used. The experiments were conducted using 1% and 1.5% CMC by weight and 1–3% HEC by weight. Pure corn syrup and 94% aqueous solutions were used as the Newtonian fluids in this study. Mixtures of 0.2–0.4% PAA by weight with pure corn syrup provided highly elastic, highly viscous fluids having a viscosity that was effectively independent of shear rate. Other concentrations and viscosity levels of the PAA solutions were obtained by adding different amounts of each concentration of the PAA into pure corn syrup. Viscosities of the Newtonian and non-Newtonian liquids were measured using a Haake Rotovisco viscometer (Model RV 12) with concentric cylinder fixtures. A calibrated glass capillary viscometer was also used to measure the viscosity of the Newtonian liquids. The surface tension of the liquids was measured by the pendant drop method. Rheological properties of Newtonian, shear thinning and viscoelastic fluids are given in Table 1.

For the case of the open end geometry, the tube or channel in most experiments was initially filled with liquid to a horizontal distance of 15 cm. The velocity of the

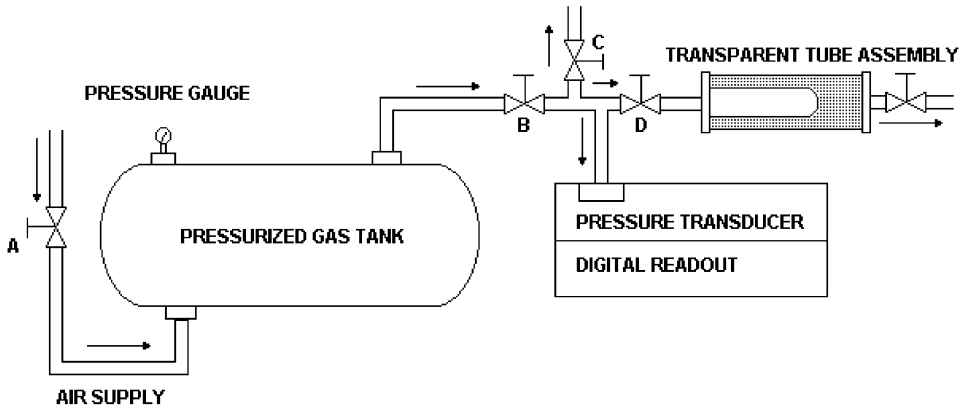

Fig. 4. Schematic diagram of the experimental apparatus.

Table 1
Rheological properties of Newtonian, shear thinning and viscoelastic fluids

Solution	Density ($g\ cm^{-3}$)	Viscosity (g/cm s)	Surface tension (dyne/cm)	Power-law index, n
1.0% HEC	0.983	7.35	65.10	0.558
2.0% HEC	0.988	93.77	71.33	0.535
3.0% HEC	0.991	492.53	43.25	0.512
1.0% CMC	0.988	16.36	80.52	0.520
1.5% CMC	0.996	163.17	51.65	0.482
100% Corn Syrup	1.342	49.66	69.05	1.00
94% Corn Syrup	1.335	15.58	101.95	1.00
10 g 0.2% PAA + 90 g Corn S.	1.325	7.45	84.95	~ 1.00
15 g 0.4% PAA + 85 g Corn S.	1.320	6.28	71.75	~ 1.00

gas bubble and the displaced liquid were determined using a stop-watch along with the observed positions of the gas–liquid interface. The moving bubble attained its final shape within a few diameters of the gas injection point and translated unchanged along the length of the tube. When one end of the tube is open to the atmosphere, the velocity of the gas bubble and liquid displaced by the gas bubble are dependent upon how much liquid lies between the nose of the bubble and the moving liquid front. In other words, the velocity is not steady. The bubble travels faster than the advancing liquid front and rapidly accelerates prior to blowout. However, the fraction of liquid deposited on the wall of the tube was assumed to be uniform and was calculated from a mass balance. The magnitude of the error involved in the approximation for each fluid is 5.97% for 1% HEC, 7.52% for 2% HEC, 8.25% for 3% HEC, 5.40% for 1% CMC, and 12.3 for 1.5% CMC solutions. These errors are calculated based on the uniform fraction of liquid obtained from a valve mounted at one end of the tube.

In addition, experiments were conducted using a completely filled tube having a 4.76 mm diameter, 50 cm length, and a valve mounted at one end. The valve provides much greater resistance than that due to liquid flow in the tube. Thus, a uniform bubble velocity along the axial direction was obtained. The maximum variation in the bubble velocity was found to be less than 5% for most of the test fluids. The capillary numbers were calculated from the average bubble velocity and viscosity at zero shear rate for shear thinning fluids. In this case, the fraction of liquid deposited on the tube wall was calculated by weighing the liquid expelled by the long gas bubble since the initial amount of liquid within the tube is known from the liquid density, tube diameter, and length.

7. Experimental results

7.1. Results for tubes open to the atmosphere

The following experimental results are for tubes open to the atmosphere unless otherwise stated. Experiments were conducted on different fluids by varying the gas pressure, the initial liquid length, and the tube radius. Each experimental condition was repeated six times in order to check repeatability. It was observed that in the CMC solutions having concentrations of 1.6% or larger, the bubble did not move in a symmetric manner along the axis of the tube or channel and the interface was not smooth. In other words, the bubble motion in the CMC solution was erratic.

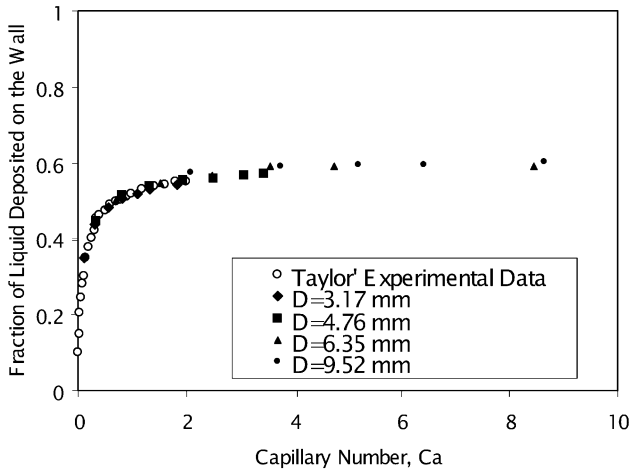

Fig. 5. The fraction of liquid deposited on the wall (m) versus capillary number for different tube diameters.

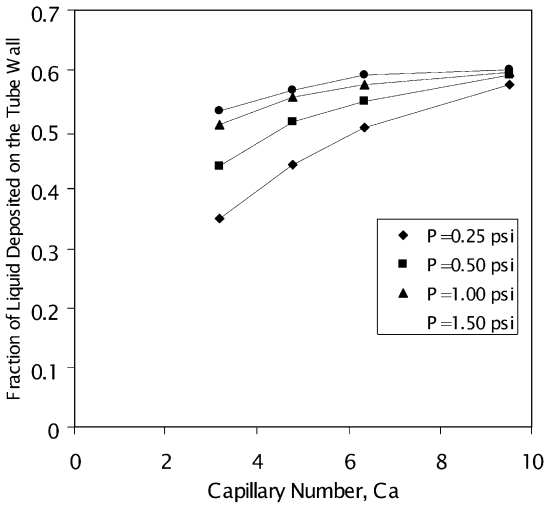

Fig. 6. The effect of tube diameter on the fraction of liquid deposited on the wall.

The fraction of Newtonian fluid (pure corn syrup) deposited on the wall for the four different diameter tubes is shown in Fig. 5 as a function of the capillary number. For the case of these open end tubes, the fractional coverage of the liquid on the tube walls is slightly higher than that reported by Taylor (1961) as can be seen in Fig. 5. This discrepancy is due to the bubble velocity variation in the axial direction since the fraction of liquid deposited on the wall depends upon the bubble velocity.

For tubes having a diameter larger than 6.35 mm gravitational effects can become significant. However, in these experiments the effect of gravity is insignificant since the blowout time is usually very short. Different capillary numbers for a particular tube and liquid are obtained by varying the pressure of the gas. The deposited film of liquid on the wall of the tube and the blowout time depend primarily on how fast the gas bubble moves through the liquid. Increasing gas pressure, shorter liquid length, larger tube radius and lower liquid viscosity reduce the flow resistance and result in higher bubble velocities and shorter blowout times.

For pure corn syrup solution (Newtonian fluid), the effect of tube diameter on the amount of liquid deposited on the wall of the tube is shown in Fig. 6 for different gas pressure levels. Similar results were obtained for the other liquids studied. As can be seen in Fig. 6, at low gas pressure the liquid fraction deposited on the wall is more sensitive to the tube diameter than at high gas pressure. In other words, the effect of tube diameter on the liquid fraction deposited on the wall gradually decreases with increasing gas pressure.

For the Newtonian fluid, the blowout length of the bubble as a function of the gas pressure is shown in Fig. 7 for different tube diameters. As expected, increasing the gas pressure decreases the blowout length. The influence of the gas pressure on the blowout length is greater for the smaller tube diameters than for the larger tube diameters.

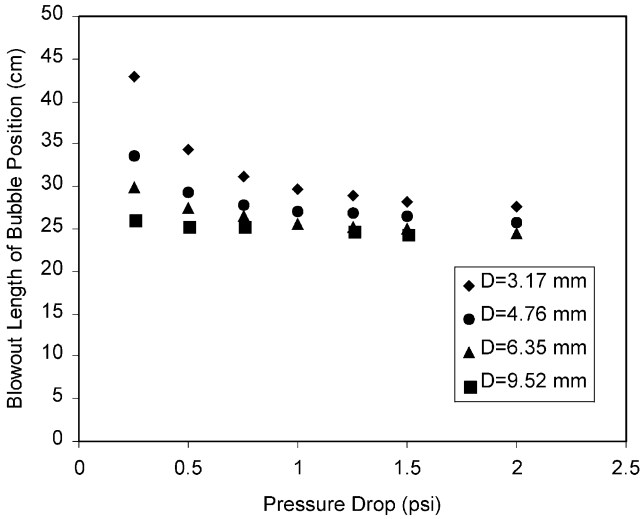

Fig. 7. Blowout length or bubble position in pure corn syrup solution as a function of the gas pressure for different tube diameters.

The fraction of liquid on the tube wall asymptotically increases to 0.565 and 0.545 for the 100% and 94% corn syrup solutions, respectively. In order to make this clear, Fig. 8 shows the liquid deposited on the wall of the tube as a function of the capillary number for one of the tubes $D = 4.76$ mm. In Fig. 8, the lower viscosity liquid starts with a low fraction of liquid deposited on the wall which increases more rapidly to its final value compared to the high viscosity liquid as the capillary number increases. However, 100% and 94% corn syrup solutions are almost identical in terms of the fraction of liquid deposited on the tube wall for a particular tube diameter as can be seen in Fig. 8.

The thickness of the liquid film deposited on the tube wall increases with increasing CMC viscosity at a higher capillary number. In order to illustrate this more clearly

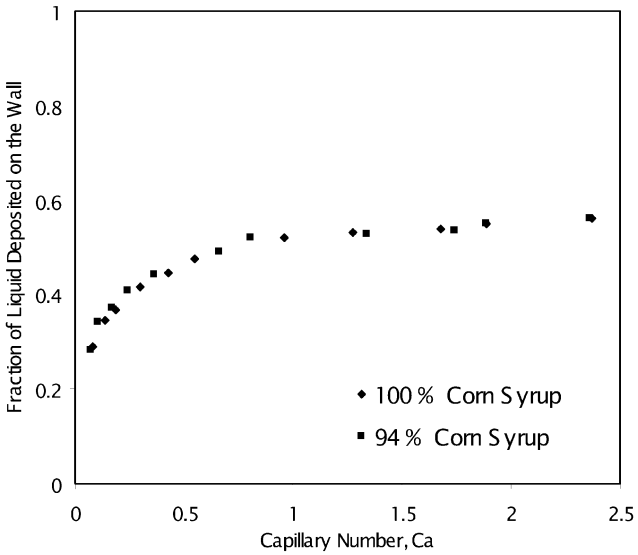

Fig. 8. The effect of viscosity of corn syrup solution on the liquid fraction on the tube wall ($D = 4.76$ mm).

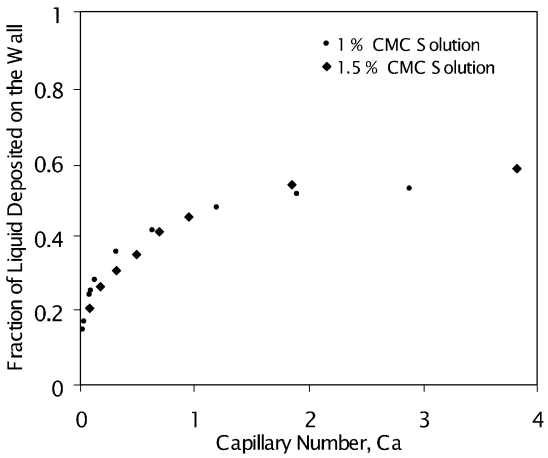

Fig. 9. The liquid fraction deposited on the tube wall as a function of capillary number for 1% and 1.5% CMC solutions ($D = 4.76$ mm).

the thickness of the liquid film deposited on the wall is plotted as a function of capillary number for one tube diameter as shown in Fig. 9. If the two CMC solutions (1% and 1.5%) are compared with each other at low capillary number, the film thickness of the 1% CMC solution is higher than that of the 1.5% CMC solution. The film thickness of the higher viscosity (shear thinning) CMC solution gradually increases with capillary number and at some point exceeds the thickness of the lower viscosity CMC solution as can be seen in Fig. 9.

Tallmadge (1969, 1970) and Spiers et al. (1975) experimentally reported and Poslinski et al. (1995) and Ro and Homsy (1995) theoretically concluded that at a low capillary number the liquid film thickness of a shear thinning liquid is lower than that of a corresponding Newtonian liquid. However, some theoretical results show that

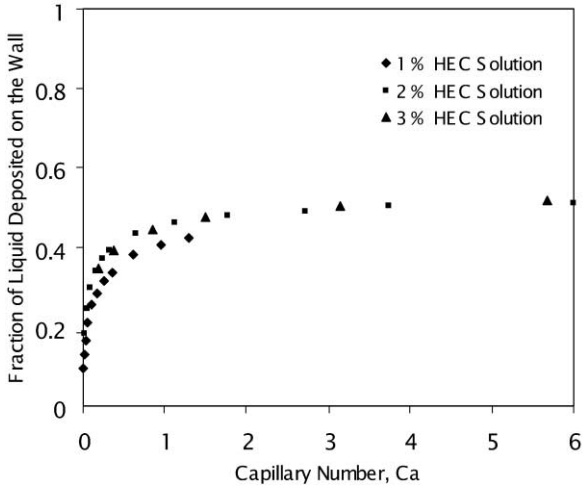

Fig. 10. The liquid fraction deposited on the tube wall as a function of capillary number for 1–3% HEC solutions ($D = 4.763$ mm).

the deposited liquid film thickness of a non-Newtonian fluid is greater than that of the corresponding Newtonian case (see Gutfinger & Tallmadge, 1965; Tallmadge, 1966, 1969; Spiers et al., 1975). The fractions of the 1–3% HEC solutions as a function of capillary number increase to about 0.48, 0.54, and 0.56, respectively. In order to examine the shear thinning effect of HEC solution, the fraction of HEC solution for a particular tube diameter 4.76 mm is plotted as a function of capillary number in Fig. 10. As can be seen in Fig. 10 the fraction of the 1–3% HEC solutions as a function of capillary number increase to about 0.48, 0.54, and 0.56, respectively.

In order to examine the effect of concentration of PAA (viscoelasticity) in pure corn syrup, three different concentrations of PAA solutions were prepared and added to pure corn syrup at three different levels. The weight percentages of PAA in the mixture (corn syrup + water + PAA) were obtained as follows: First, 0.2–0.4% wt aqueous PAA stock solutions were prepared. Different amounts of these PAA solutions were added to corn syrup as shown in Table 2. The liquid fraction deposited on the tube wall increases with increasing viscoelasticity of polymer solution. Fig. 11 shows the effect of viscoelasticity of polymer solution for experiments conducted using a particular diameter tube. Higher viscoelasticity (polymer concentrations) result in a thicker fraction of liquid deposited on the tube wall at almost all values of capillary numbers. The effect of the viscoelastic behavior of fluid by changing solvent nature on the liquid film thickness was examined. The mixture (water + corn syrup + PAA) viscoelasticity for a constant amount of corn syrup increases with an increasing amount of PAA. In order to examine the effect of the mixture viscosity, two different 0.02% and 0.03% PAA solutions were prepared by adding different amounts of corn syrup as shown in Table 2. The fraction of these solutions deposited on the tube wall as a function of capillary number is shown in Fig. 11 for a

Table 2
Preparation of PAA solutions with corn syrup

Mixture	% Corn syrup	% Water	% PAA
5 g 0.2% solution + 95 g corn syrup	95	4.990	0.010
10 g 0.2% solution + 90 g corn syrup	90	9.980	0.020
15 g 0.2% solution + 85 g corn syrup	85	14.930	0.030
5 g 0.3% solution + 95 g corn syrup	95	4.985	0.015
10 g 0.3% solution + 90 g corn syrup	90	9.970	0.030
15 g 0.3% solution + 85 g corn syrup	85	14.955	0.045
5 g 0.4% solution + 95 g corn syrup	95	4.980	0.020
10 g 0.4% solution + 90 g corn syrup	90	9.960	0.040
15 g 0.4% solution + 85 g corn syrup	85	14.940	0.060

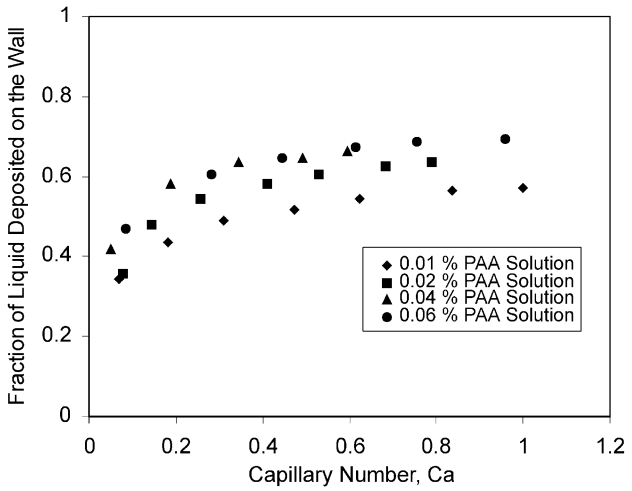

Fig. 11. The effect of viscoelasticity (PAA concentration) on the liquid fraction deposited on the wall as a function of capillary number ($D = 4.76$ mm).

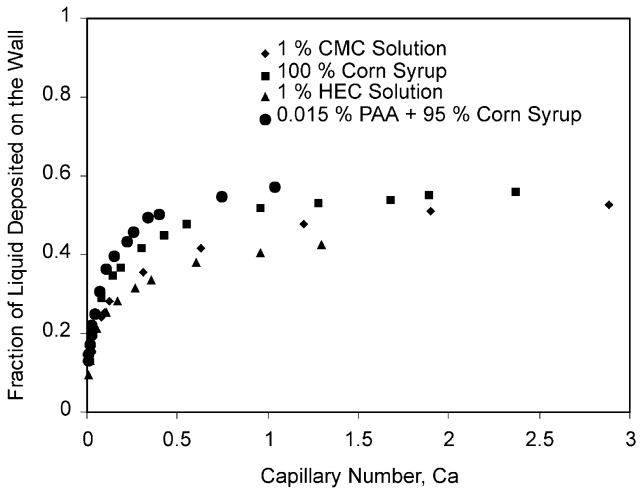

Fig. 12. The liquid fraction deposited on the tube wall as a function of capillary number for Newtonian, shear thinning, and viscoelastic fluids ($D = 4.76$ mm).

particular diameter tube. As can be seen in this figure, the effect of the viscoelastic behavior of the fluid by changing solvent nature on the liquid film thickness increases with increasing viscoelasticity (polymer concentration).

7.2. Results for a valve-mounted tube

As stated previously, when the valve is mounted at one end of a tube, the bubble velocity becomes independent of the amount of liquid between the bubble front and the valve since the valve provides much more resistance than that due to flow. Thus, a uniform bubble velocity in the axial direction can be obtained in this arrangement. In order to compare the results of the open tube with that of the valve-mounted tube, experiments were performed using one particular tube diameter ($D = 4.76$ mm). The fraction of liquid deposited on the wall as a function of capillary number is shown in Fig. 12. In this figure, the fractions of different liquids deposited on the tube wall are compared with one another. As can be seen in the figure, the amount of residual viscoelastic fluid (95% corn syrup + 0.015% PAA solution) is larger than that of a Newtonian fluid (pure corn syrup) and shear thinning fluids (1% HEC and 1% CMC solutions). Similar results were obtained using the open end tube (see Kamışlı, 1997 for more detail). The only difference between these results is that the amount of residual liquid on the tube wall for the open tube is larger than that compared to the corresponding valve-mounted tube. Boger fluids behave nearly identically to the Newtonian fluids at a low capillary number. This result is expected since the Boger fluids have nearly constant shear viscosity and since the elasticity of the Boger fluids (in the absence of shear thinning) should not be important at low shear rates. However Boger fluids exhibit high levels of elasticity at large strain rates (see Huzyak & Koelling, 1997). Thus, it is possible to conclude that increase in fractional coverage at high strain rates, corresponding to high capillary numbers, is due to the elasticity of Boger fluids.

Fig. 9 gives the fractional coverage of 1% and 1.5% CMC solutions as a function of capillary number. The fraction of 1% CMC solution deposited on the wall is larger than that of the 1.5% CMC solution at a low capillary number. Similar results were obtained for the open tube. Ro and Homsy (1995) theoretically examined the effect of shear thinning on the film thickness on the wall

of the rectangular channel. They concluded that "The weakening of the viscous shear stress especially near the wall due to shear thinning decreases the efficiency of the momentum transfer from the plate to the shear thinning fluid, resulting in a lower amount of fluid being pulled out to form films. The effect of normal stress thinning is to lessen the film thinning action of the normal stress. Also in their study, it has been shown that the horizontal gradient of the xx normal stress creates forces that tend to lower the film thickness by resisting the stretching action of the plate. Therefore, weakening of the horizontal normal stress reduces the resistance to axial extension and raises the film thickness". In the light of the above explanation, it may be concluded that at a low capillary number, corresponding to low strain rates, 1% CMC solution shows less shear thinning than that of 1.5% CMC solution. At a high capillary number the normal stress thinning becomes more important than shear stress thinning for CMC solutions.

The fractional coverage of the HEC solutions (1–3% HEC) are compared in Fig. 10. As can be seen in the figure, the fractional coverage of the liquid increases with an increase in shear thinning effect of HEC or liquid viscosity at a high capillary number. Similar results are numerically obtained by Poslinski and Coyle (1994). They have performed numerical simulation of gas-assisted displacement in a tube using a viscosity model which included shear thinning effects. Numerical results showed that fluids with a shear thinning viscosity exhibit a smaller fractional coverage than a Newtonian fluid at the same capillary number. Fractional coverage was also found to be smaller for a fluid with a smaller shear thinning index.

As mentioned earlier, the fractional coverage of the fluid for a valve-mounted tube is less than that of the corresponding open tube. These results are expected since the amount of residual liquid deposited on the tube wall depends very much upon the bubble velocity. During gas-assisted displacement in an open tube, the bubble velocity increases as the amount of liquid between the bubble front and liquid front decreases. Therefore, the fractional coverage for the open tube is expected to be higher than that of the valve-mounted tube.

7.3. Results and discussion

A simple analysis based on a power-law model of a non-Newtonian fluid was compared with the results of Poslinski et al. (1995). The Newtonian analysis of Poslinski et al. (1995) may be obtained from the present results when the power-law index n is taken to be 1. The relative bubble front and liquid front position with respect to the blowout length are shown in Fig. 3a as a function of the relative time to blowout for different values of n. As can be seen in Fig. 3a the bubble front position is retarded with decreasing power-law index which is equivalent to lower gas pressure, longer liquid length or smaller radius, thereby resulting in a thinner coating thickness. The thinner coating thickness corresponds to a larger amount of liquid being displaced, additional flow resistance, and an impedance to gas penetration. The same result can be seen in Fig. 3b. The relative bubble velocity with respect to the initial bubble velocity decreases with decreasing n until close to blowout ($t/t_b \approx 0.85$). Since the fraction of liquid deposited on the walls depends very much upon the bubble velocity, low bubble velocity corresponds to a smaller liquid fraction on the walls. This result qualitatively agrees with the experimental data obtained by Tallmadge (1969, 1970) and Spiers et al. (1975) for free coating on a vertically withdrawn plate from a liquid bath. The velocities of the liquid front and the bubble front increase slowly during the early stages of displacement and rise rapidly later ($t/t_b \approx 0.85$). The relative bubble and liquid velocities decrease with decreasing power-law index until around $t/t_b \approx 0.85$ and after this point these quantities increase with decreasing n as shown in Fig. 3b. In other words, the bubble accelerates more rapidly in a shear thinning fluid at later times ($t/t_b \approx 0.85$). This is also in agreement with the numerical results of Poslinski et al. (1995) in which viscoplastic liquids are modeled by means of a Buckingham–Reiner expression. Based on the experimental observations it appears that a simple model successfully captures the gas–liquid dynamics for Newtonian and non-Newtonian fluid displacement in a tube and channel. As can be seen in Fig. 3b the relative liquid velocity is always slower than the relative bubble front velocity. The bubble velocity exceeds the initial or average bubble velocity at $t/t_b \approx 0.75$ (depending on the value of the power-law index).

In the experimental study, the effects of viscoelasticity and shear thinning effect on the fraction of liquid deposited on the tube wall has been experimentally examined. It is concluded that while viscoelastic fluids (corn syrup + PAA solutions) give higher fractional coverage compared to corresponding Newtonian fluids (pure corn syrup) the shear stress thinning fluids (1% CMC, 1 and 2% HEC) give lower fractional coverage compared to corresponding Newtonian fluids. However, an increase in shear stress thinning (concentration of CMC and HEC) results in higher fractional coverage at a higher capillary number. Thus, a higher fractional coverage of the shear thinning fluid compared to the corresponding Newtonian fluid was obtained by increasing the concentration of CMC (a small change in concentration results in a large change in viscosity) at a higher capillary number.

As mentioned previously, the reduced fraction of liquid deposited on the walls of a tube or channel results in a larger amount of liquid being displaced, adding to the flow resistance, and thus impeding the gas penetration. Also the horizontal gradient of the axial normal stress creates forces that tend to lower the film thickness by resisting the stretching action of the walls of the tube or

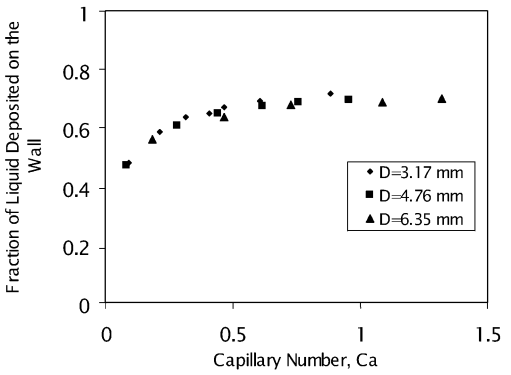

Fig. 13. The liquid fraction deposited on the wall as a function of capillary number for 0.06% PAA + 85% corn syrup ($D = 4.763$ mm).

channel. Therefore, the weakening of the horizontal normal stress reduces the resistance to axial extension, and raises the film thickness. On the other hand, the weakening of the viscous shear stress, especially near the wall of the tube or channel, due to shear thinning decreases the efficiency of momentum transfer from the wall to the viscoelastic fluid, resulting in a lower amount of residual fluid being deposited on the wall.

In order to examine the effect of viscoelasticity alone on the liquid fraction deposited on the wall as a function of capillary number, three different concentrations of PAA solutions were prepared and added to pure corn syrup at three different levels. The detailed results of the experiments are given in the previous section. These mixtures (corn syrup + PAA + water) do not exhibit shear stress thinning (Boger fluids). Huzyak and Koelling (1994) reported that the fractional coverage of a Boger fluid (0.31 wt% high molecular weight polyisobutylene ($Mw = 1.2 \times 10^6$) + 4.97 wt% hydrocarbon solvent, tetradecane + 94.72 wt% low molecular weight polybutene ($Mw = 10^3$)) deposited on the tube wall asymptotically increased and reached a value of 0.75 with increasing capillary number. As can be seen in Fig. 13, for 0.06 wt% + 85 wt% corn syrup, the liquid fraction deposited on the tube wall is approximately 0.70. This value of residual liquid fraction qualitatively agrees with the asymptotic value of Huzyak and Koelling (1994). It cannot be compared quantitatively since the test fluids used in each experiment are different from one another.

From a comparison of the fractional coverage of the polymer (PAA) added to corn syrup solutions (Boger fluids) with that of pure corn syrup solutions (Newtonian fluid) as a function of capillary number, the Boger fluids yield a thicker residual liquid fraction as compared to the corresponding pure corn syrup solutions at a large capillary number. This result is expected since polymers added to corn syrup solutions at low concentrations exhibit elastic behavior but do not exhibit shear thinning. Some of the liquid retracts due to fluid elasticity and influences fractional coverage when a long gas bubble displaces an elastic fluid (Boger fluid). Therefore, elastic fluids (in the absence of shear thinning) result in a higher liquid fraction deposited on the wall as a function of the capillary number as compared with corresponding Newtonian fluids.

7.4. Conclusions

The experiments indicate that the fraction of non-Newtonian liquid deposited on the tube wall depends very much upon the fluid rheology. Thus, it is difficult to make general quantitative statements which are valid for all non-Newtonian fluids. For instance, although the residual fraction of 1% and 1.5% CMC solutions at a lower capillary number is thinner than that of Newtonian fluid, at a higher capillary number the fractional coverage of these solutions increase and approach 0.62 and 0.69, respectively. On the other hand, the residual fraction of 1% and 2% HEC solutions increase and approach 0.48 and 0.545, respectively.

Polymer (PAA) added to corn syrup solutions (Boger fluids) results in a thicker residual liquid fraction deposited on the wall as a function of capillary number compared to that of a corresponding Newtonian fluid. For 0.06 wt% + 85 wt% corn syrup the residual liquid fraction as a function of capillary number asymptotically increases and approaches a value of 0.70.

It was observed that the fractional coverage of a liquid on the wall of a tube open to the atmosphere is larger than that of a corresponding valve-mounted closed tube. Increasing pressure results in shorter blowout times and increased liquid film thickness.

The simple model developed for the case of a power-law fluid successfully captures the gas–liquid dynamics for both Newtonian and non-Newtonian fluid displacement in a tube or channel. The prediction of the liquid fraction deposited on the wall qualitatively agrees with the experimental observations.

For non-Newtonian inelastic fluids, shear stress thinning behavior results in reduced liquid film thickness.

References

Bretherton, F. P. (1961). The motion of long bubbles in tube. *Journal of Fluid Mechanics*, *10*, 166–188.

Chang, R. Y., Tsai, M. H., & Hsu, C. H. (1997). On the dynamics of gas-assisted injection molding process. *SPE Technical Papers*, *43*, 598–602.

Chen, S. C., Hu, S. Y., Jong, W. R., & Jeng, M. C. (1997). Structural analysis, process simulation and warpage calculation for the gas-assisted injection molding parts using unified CAE model. *SPE Technical Papers*, *43*, 620–624.

Cox, B. G. (1962). On driving a viscous fluid out of a tube. *Journal of Fluid Mechanics*, *14*, 81–96.

Cox, B. G. (1964). An experimental investigation of the streamlines in viscous fluid expelled from a tube. *Journal of Fluid Mechanics*, *20*, 193–200.

Fairbrother, F., & Stubbs, A. E. (1935). Studies in electroendosmosis. Part VI. The bubble-tube methods of measurements. *Journal of Chemical Society*, *1*, 527.

Friedrichs, B., & Güç eri, S. I. (1993). A novel hybrid numerical technique to model 3-D fountain flow in injection molding processes. *Journal of Non-Newtonian Fluid Mechanics*, *49*, 141–173.

Huzyak, P. C., & Koelling, K. W. (1994). Gas bubble penetration through viscoelastic fluids. Paper presented at International Conference on Gas-Assisted Injection Molding Technology, OH: Ohio State University.

Huzyak, P. C., & Koelling, K. W. (1997). The penetration of a long bubble through a viscoelastic fluid in a tube. *Journal of Non-Newtonian Fluid Mechanics*, *175*, 73–88.

Gutfinger, C., & Tallmadge, J. A. (1965). Films of Non-Newtonian fluids adhering to flat plates. *A.I.Ch.E.*, *11*, 403–413.

Kamal, M. R., Goyal, S. K., & Chu, E. (1988). Simulation of injection mold filling of viscoelastic polymer with fountain flow. *A.I.Ch.E.*, *34*, 94–106.

Kamışlı, F. (1997). Mathematical analysis and experimental study of gas-assisted injection molding. Ph.D. Dissertation, State University of New York at Buffalo.

Koelling, K. W., & Kaminski, R. C. (1996). Gas-assisted injection molding: Influence of processing conditions and material properties. *SPE Technical Papers*, *42*, 644–648.

Kolb, W. B., & Cerro, R. L. (1991). Coating the inside of a capillary of square cross-section. *Chemical Engineering Science*, *46*, 2181–2195.

Kolb, W. B., & Cerro, R. L. (1993). The motion of long bubbles in tubes of square cross-section. *The Physics of Fluids A*, *5*, 1549–1557.

Landau, L. D., & Levich, V. G. (1942). Dragging of a liquid by a moving plate. *Acta Physicochimica URSS*, *17*, 42.

Marchessault, R. H., & Mason, S. G. (1960). Flow of entrapped bubbles through a capillary. *Industrial Engineering Chemistry*, *52*, 79–84.

McLean, J. M., & Saffman, P. G. (1981). The effect of surface tension on the shape of fingers in a Hele–Shaw cell. *Journal of Fluid Mechanics*, *102*, 455–469.

Moritzer, E., & Potente, H. (1996). Theoretical and practical results for the gas injection molding process variant: Melt displacement into an overflow cavity. *SPE Technical Papers*, *42*, 674–678.

Park, C. W., & Homsy, G. M. (1984). Two-phase displacement in Hele–Shaw cell: Theory. *Journal of Fluid Mechanics*, *139*, 291–308.

Pitts, E. J. (1980). Penetration offluid into a Hele–Shaw cell: The Saffman–Taylor Experiment. *Fluid Mechanics*, *97*, 53–64.

Poslinski, A. J., & Coyle, D. J. (1994). Steady gas penetration through non-Newtonian liquids in tube and slit geometries: isothermal shear thinning effects. *Proc. Polymer Processing Society*, *10th Annual Metting*, p. 219.

Poslinski, A. J., Oehler, P. R., & Stokes, V. K. (1995). Isothermal gas-assisted displacement of viscoplastic liquids in tubes. *Polymer Engineering and Science*, *35*, 877–895.

Ratulowski, J., & Chang, H. C. (1989). Transport of the gas bubbles in capillaries. *The Physics of Fluids A*, *1*, 1642–1655.

Reinelt, D. A., & Saffman, P. G. (1985). The penetration of a finger into a viscous fluid in a channel and tube. *SIAM Journal of Science and Statistical Computers*, *6*, 542–561.

Reinelt, D. A. (1987a). The effect of thin film variations and transverse curvature on the shape of fingers in Hele–Shaw cell. *The Physics of Fluids*, *30*, 2617–2623.

Reinelt, D. A. (1987b). Interface conditions for two-phase displacement in Hele–Shaw cell. *Journal of Fluid Mechanics*, *183*, 219–234.

Ro, J. S., & Homsy, G. M. (1995). Viscoelastic free surface flows: Thin film hyrodynamics of Hele–Shaw and dip coating flows. *Journal of Non-Newtonian Fluid Mechanics*, *57*, 203–225.

Saffman, P. G., & Taylor, G. I. (1958). The penetration of a fluids into a porous medium or Hele–Shaw cell containing a more viscous liquid. *Proceedings of Royal Society of London*, *A 245*, 312–329.

Schwart, L. W., Princen, H. W., & Kiss, A. D. (1986). On the motion of bubbles in capillary tubes. *Journal of Fluid Mechanics*, *172*, 259–275.

Shen, E. I., & Udell, K. S. (1985). A finite element study of low Reynolds number two phase flow in cylindrical tubes. *Transactions of the ASME E: Journal of Applied Mechanics*, *52*, 253–256.

Spiers, R. P., Subbaraman, C. V., & Wilkinson, W. L. (1975). Free coating of Non-Newtonian liquids onto a vertical surface. *Chemical Engineering Science*, *30*, 379–395.

Tabeling, P., Zocchi, G., & Libchaber, A. (1987). An experimental study of the Saffman–Taylor instability. *Journal of Fluid Mechanics*, *177*, 67–82.

Soh, Y. S., & Chung, C. H. (1997). Flow directions in the gas-assisted injection molding technology. *SPE Technical Papers*, *43*, 603–609.

Tallmadge, J. A. (1966). A withdrawal theory for Ellis model fluids. *A.I.Ch.E.*, *12*, 1011–1014.

Tallmadge, J. A. (1969). A variable-coefficient plate withdrawal theory for power-law fluids. *Chemical Engineering Science*, *24*, 471–480.

Tallmadge, J. A. (1970). Withdrawal of flat plates from power-law fluids. *A.I.Ch.E.*, *16*, 925–930.

Turng, L. S., & Wang, V. W. (1991). Simulation of coinjection and gas-assisted injection molding process. *SPE Technical Papers*, *37*, 297–300.

Turng, L. S. (1993). New developments in CAE technology for the gas-assisted injection molding process. *SPE Technical Papers*, *39*, 74–78.

Taylor, G. I. (1961). Cavitation of a viscous fluid in narrow passages. *Journal of Fluid Mechanics*, *10*, 161–165.

Westborg, H., & Hassager, O. J. (1989). Creeping motion of long bubbles and drops in capillary tubes. *Colloid Interface Science*, *133*, 135–147.